Petroleum Research 11 (2026) 206–216

Contents lists available at ScienceDirect

Petroleum Research

journal homepage: http://www.keaipublishing.com/en/journals/petroleum-research/

Full Length Article

Numerical simulation of microbial biohydrogen production under high-pressure, high-temperature conditions for enhanced recovery from depleted reservoirs

David Abutu [a,c], Peter Ikechukwu Nwaichi [a], Chika Umunnawuike [a], Francis Nyah [a], Barima Money [a], Hafizuddin Wan Yussof [a], Augustine Agi [a,b,*]

[a] Faculty of Chemical and Process Engineering Technology, Universiti Malaysia Pahang Al-Sultan Abdullah, Lebuhraya Persiaran Tun Khalil Yaakob 26300 Kuantan, Pahang, Malaysia
[b] Centre for Research in Advanced Fluid and Processes (Fluid Centre), Universiti Malaysia Pahang Al-Sultan Abdullah, 26300 Gambang, Pahang, Malaysia
[c] Department of Chemical Engineering, Federal University Wukari, Nigeria

ARTICLE INFO

Article history:
Received 15 February 2025
Received in revised form
24 July 2025
Accepted 27 July 2025
Available online 6 August 2025

Keywords:
Depleted hydrocarbon reservoir
Dark fermentation
Biohydrogen
Bioreactor simulation
High temperature high pressure bioreactor

ABSTRACT

The growing demand for sustainable energy has intensified interest in biohydrogen production under extreme environmental conditions. This study presents a numerical simulation of hydrogen production in a high-temperature, high-pressure batch bioreactor system designed to mimic depleted hydrocarbon reservoir environments. The model captures microbial fermentation dynamics using dual substrates glucose and *n*-hexadecane under varying temperature (35–70 °C), pressure (1–40 atm), salinity (0–50 g/L NaCl), and surfactant-enhanced availability ($\alpha = 1$–12). Monod kinetics with product (Hydrogen) and salinity inhibition terms govern biomass growth and substrate consumption. Gas accumulation is modeled using Henry's and ideal gas laws, while thermal behavior is represented using lumped heat transfer and Arrhenius-based growth scaling. Initial conditions include 10 mmol/L glucose, 1 mmol/L hexadecane, and 0.1 g/L biomass in a 1.0 L batch system at 55 °C. Over 24 h, the model predicts a maximum hydrogen accumulation of 4.34 L, with a final H_2 purity of 89.6% and biomass concentration of 1.20 g/L. Parametric simulations reveal that 55 °C yields the highest hydrogen output (3.31 mol/mol substrate), while increasing salinity and pressure reduce biomass and gas evolution. Surfactant addition significantly improves hydrocarbon utilization, reducing hexadecane from 1.0 to 0.12 mmol/L at $\alpha = 12$, with up to 72.8% yield enhancement. Glucose drives early hydrogen evolution, while hexadecane contributes to sustained production under co-metabolic conditions. All equations were solved using Python with parametric looping and ODE integration. This simulation framework provides a robust tool for evaluating microbial-enhanced hydrogen recovery (MEHR) and optimizing reactor design conditions for biohydrogen generation in repurposed subsurface reservoirs.

© 2025 Chinese Petroleum Society. Publishing services by Elsevier B.V. on behalf of KeAi Communications Co. Ltd. This is an open access article under the CC BY-NC-ND license (http://creativecommons.org/licenses/by-nc-nd/4.0/).

1. Introduction

Hydrogen is increasingly recognized as a key enabler of the global transition toward low-carbon energy systems (Umunnawuike et al., 2024). Among the various production methods, biological hydrogen production via dark fermentation offers a sustainable and scalable alternative that utilizes organic substrates such as carbohydrates, waste biomass, and even hydrocarbons under anaerobic conditions (Goria et al., 2022; Jain et al., 2024). This microbial process is typically powered by thermophilic or halophilic consortia, which can metabolize substrates at elevated temperatures (≥50 °C) and high salinity conditions commonly found in depleted oil and gas reservoirs (Gupta et al., 2024). As a result, these subsurface formations have been proposed as promising geobiological environments for in situ hydrogen generation using tailored microbial systems.

* Corresponding author. Faculty of Chemical and Process Engineering Technology, Universiti Malaysia Pahang Al-Sultan Abdullah, Lebuhraya Persiaran Tun Khalil Yaakob 26300 Kuantan, Pahang, Malaysia
E-mail address: augustine@umpsa.edu.my (A. Agi).
Peer review under the responsibility of Editorial Office of Petroleum Research.

https://doi.org/10.1016/j.ptlrs.2025.07.006
2096-2495/© 2025 Chinese Petroleum Society. Publishing services by Elsevier B.V. on behalf of KeAi Communications Co. Ltd. This is an open access article under the CC BY-NC-ND license (http://creativecommons.org/licenses/by-nc-nd/4.0/).

To visualize this concept, Fig. 1 presents a schematic overview of microbial hydrogen production within a depleted hydrocarbon reservoir. Here, residual oil components (e.g., *n*-alkanes) serve as carbon sources, either alone or in co-metabolism with simpler substrates like glucose or organic rich wastewater. Hydrogen produced via microbial metabolism accumulates in the pore space and can be recovered using existing well infrastructure (Vilcáez and Chowdhury, 2025). This approach often referred to as microbial enhanced hydrogen recovery (MEHR) could convert unused reservoirs into low-carbon energy assets while avoiding land and infrastructure costs associated with surface bioreactors.

Despite the growing interest in MEHR, current experimental studies are largely limited to ambient-pressure, serum-bottle systems that do not capture the thermodynamic and transport conditions of real reservoirs. For instance, Veshareh et al. (2022) demonstrated hydrogen production from *n*-hexadecane and crude oil using *Thermotoga* strains at 60–70 °C. However, their experiments were conducted in sealed vials under atmospheric pressure, without simulating reservoir-relevant parameters such as hydrostatic pressure (up to 40 atm), salinity (up to 50 g/L NaCl), or diffusion-limited mass transfer (Veshareh et al., 2022). As a result, there remains a clear gap in understanding the behavior of microbial fermentation systems under subsurface-relevant conditions.

To address this gap, the present study develops a numerical simulation model of hydrogen production in a virtual high-pressure, high-temperature batch bioreactor designed to mimic the thermophysical environment of depleted reservoirs. The simulation includes dual-substrate fermentation using glucose and *n*-hexadecane, with the latter's limited solubility addressed through a surfactant enhancement factor based on Veshareh's reported 12 × yield improvement. The microbial kinetics are governed by Monod models with inhibition terms for hydrogen partial pressure and salinity, while thermal response is modeled using Arrhenius-based correction and convective heat loss. Gas-phase accumulation follows Henry's and ideal gas laws to track headspace hydrogen volume and purity (Nadal-Rey et al., 2022).

Fig. 2 presents the hypothetical flow diagram of the batch bioreactor system modeled in this study, including key elements such as substrate input, microbial growth, hydrogen generation, and gas accumulation. The reactor can be pressurized with Nitrogen gas and temperature maintained with heating element to mimic reservoir condition. All simulations were implemented in Python using parametric loops over temperature (35–70 °C), pressure (1–40 atm), salinity (0–50 g/L), and surfactant factor ($\alpha = 1$–12), producing time-resolved outputs for biomass, substrate degradation, and hydrogen evolution. This framework offers a scalable and reproducible tool for pre-screening bioreactor conditions and supports the long-term feasibility of deploying microbial hydrogen production strategies in real geological formations. In doing so, it advances the field beyond lab-scale observations toward practical, field-informed system design.

2. Methodology

2.1. Overview of simulation approach

This study adopts a numerical modeling approach to simulate biohydrogen production under high-pressure, high-temperature, and saline conditions representative of depleted hydrocarbon reservoirs. Instead of fabricating a physical bioreactor, the entire system was implemented as a mathematical model coded in Python. This approach enables a parametric understanding of how key environmental variables including temperature, pressure, salinity, and surfactant-enhanced substrate availability affect hydrogen yield and microbial performance in anaerobic systems.

The simulation is structured around solving a set of coupled ordinary differential equations (ODEs) that describe biomass growth, substrate consumption, hydrogen generation, and energy balance. These equations are parameterized with biologically relevant constants extracted from literature and calibrated against experimental studies such as Veshareh et al. (2022) for hexadecane fermentation and Gupta et al. (2024) for thermophilic glucose fermentation. By integrating both substrates into a dual-pathway fermentation model, the simulation captures co-metabolism and substrate interaction effects that are often observed in microbial consortia.

The simulation environment assumes a batch bioreactor operating under reservoir-like conditions, including anaerobic operation, static liquid phase (no agitation), and external temperature control. This allows for a realistic approximation of subsurface constraints such as diffusion-limited mass transfer and thermodynamic feedbacks. Simulations were conducted over 24-h periods to reflect complete batch cycles, with outputs evaluated across multiple operating conditions to assess performance trends and optimize system parameters for potential field deployment.

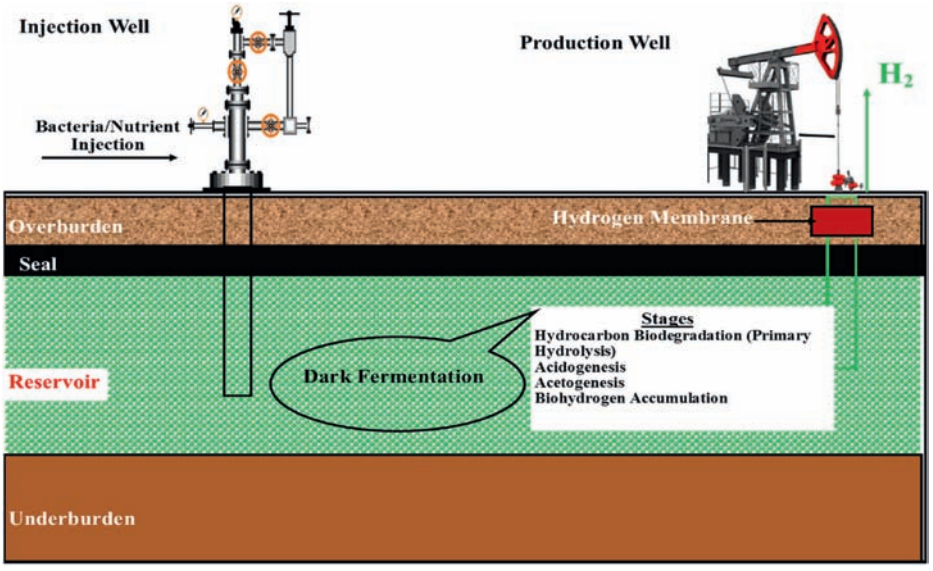


Fig. 1. Conceptual illustration of biohydrogen production in depleted hydrocarbon reservoir.

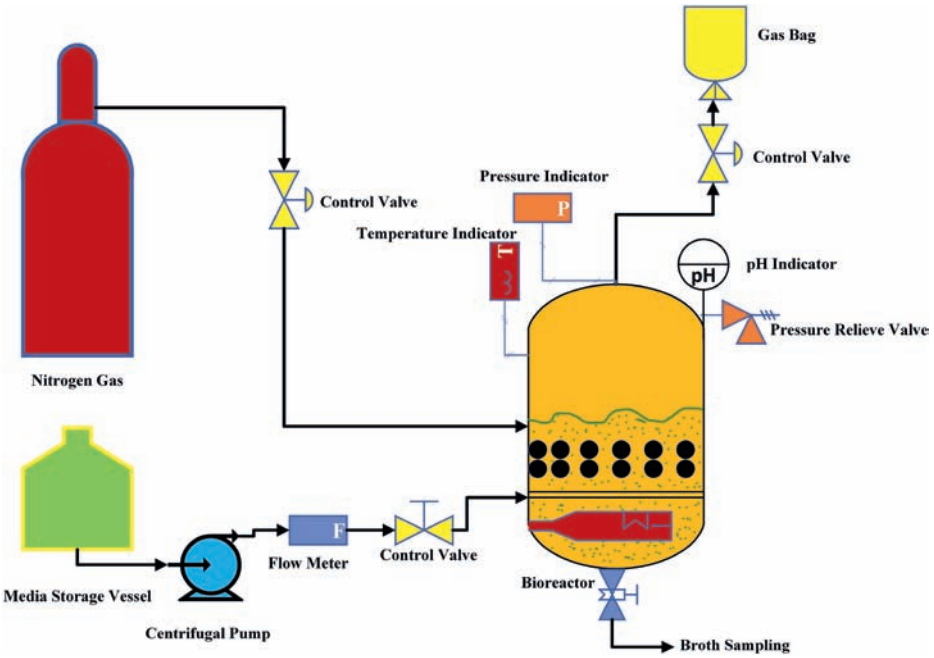


Fig. 2. Hypothetical flow diagram of the simulated batch bioreactor system.

2.2. Microbial kinetics and reaction modeling

Microbial growth and hydrogen production in the simulation are modeled using Monod-type kinetics with substrate-specific and environmental inhibition terms. The Monod equation relates the specific growth rate (μ) to substrate concentration, reflecting saturation-limited microbial behavior. For glucose and *n*-hexadecane, independent substrate consumption equations are modeled, each scaled by the respective yield coefficients and growth rates. The glucose pathway primarily supports rapid biomass generation, while hexadecane provides sustained hydrogen production through slower hydrocarbon degradation. This dual-substrate strategy mimics co-metabolism behavior observed in mixed cultures, such as *Thermotoga* and *Clostridium* species (Sarangi and Nanda, 2020; Ziara et al., 2019).

The complete growth rate expression incorporates inhibition by hydrogen partial pressure and salinity, two key constraints in subsurface environments. Hydrogen accumulation in the reactor headspace reduces fermentation efficiency by inhibiting hydrogenase activity, a well-documented effect in dark fermentation. This is modeled using a non-competitive inhibition term as shown in equation (1) (Medina et al., 2024; Wu et al., 2024):

$$\mu = \mu_{max}\frac{S}{K_S + S}\ \frac{1}{1+\frac{P_{H_2}}{K_I^P}}\ \frac{1}{1+\left(\frac{C_{NaCl}}{K_I^{Salt}}\right)^n} \tag{1}$$

Where μ is the effective growth rate (h^{-1}), S_{eff} is the effective substrate concentration (mol/L), K_s is the half-saturation constant, P_{H2} is the hydrogen partial pressure (atm), C_{NaCl} is the salinity (g/L), and K_I^{Salt} and K_I^p are inhibition constants. The exponent n captures non-linearity in salinity inhibition, typically set to 2 for osmotic stress modeling. This equation enables simulation of growth deceleration under adverse environmental conditions reported in halophilic and thermophilic systems (Imai, 2024).

Substrate degradation is directly linked to microbial growth through yield coefficients $Y_{X/S}$ (Equation (2)), while hydrogen production is calculated using substrate-specific hydrogen yields $Y_{H2/S}$ (Equation (3)). For co-metabolism, total hydrogen production is the sum of contributions from glucose and hexadecane degradation (Equation (4)) which is directly linked to biomass growth via the yield coefficient $Y_{X/S}$.

$$\frac{dS}{dt} = \frac{1}{Y_{X/S}}\ .\mu.X \tag{2}$$

$$\frac{dH_2}{dt} = Y_{H_2/S}.\left(-\frac{dS}{dt}\right) \tag{3}$$

$$\frac{dH_2}{dt} = Y_{H_2/G}.\left(-\frac{dG}{dt}\right) + \frac{dH_2}{dt} = Y_{H_2/H}.\left(-\frac{dH}{dt}\right) \tag{4}$$

where G and H refer to glucose and hexadecane concentrations. The simulation accounts for nonlinear dynamics where glucose supports initial biomass proliferation, thereby enhancing enzymatic access to hexadecane, a phenomenon supported by Veshareh et al. (2022).

2.3. Thermodynamic and gas phase modeling

To simulate hydrogen accumulation and gas-phase behavior in the reactor, thermodynamic relationships are incorporated using Henry's law and the ideal gas law (Equation (5)). Hydrogen produced via microbial metabolism is assumed to instantaneously partition into the gas phase. The equilibrium concentration of dissolved hydrogen in the liquid phase can be evaluated using equation (5) (Kaydouh and El Hassan, 2022; Li et al., 2024).

$$C_{H_2}^{liquid} = H_c(T).\ P_{H_2} \tag{5}$$

where Hc(T) is the temperature-dependent Henry's constant (mol/L·atm) and P_{H2} is the partial pressure of hydrogen in the headspace. The relationship between gas-phase hydrogen concentration and liquid inhibition allows feedback from gas accumulation

to impact biological kinetics (Kaydouh and El Hassan, 2022). The total volume of hydrogen gas accumulated in the reactor headspace is estimated using the ideal gas law (Equation (6)):

$$V_{H_2} = \frac{nH_2 . RT}{P} \quad (6)$$

Here, n_{H2} is the number of moles of hydrogen, R is the universal gas constant (0.0821 L atm/mol·K), T is the absolute temperature, and P is the operating pressure. This allows direct calculation of gas volume under varying reactor conditions, enabling purity estimates when total gas composition is considered. Pressure-dependent inhibition is linked back into microbial kinetics through the P_{H2} term, creating a thermodynamic-biological feedback loop. The model assumes no hydrogen loss from the system (closed batch) and instantaneous equilibrium between gas and liquid phases assumptions that reflect static reservoir-like conditions with limited mass transfer.

2.4. Heat transfer and temperature dynamics

To account for reactor thermal behavior under subsurface-mimicking conditions, the model includes a lumped-parameter energy balance that simulates temperature change within the reactor volume. Given that microbial heat production is negligible compared to external heating input, the primary driver of temperature dynamics is heat exchange with the surrounding environment. This is modeled using Newton's law of cooling (Equation (7)) (Aghajani Delavar and Wang, 2022; Basak et al., 2022).

$$\rho C_p \frac{dT}{dt} = \frac{Q}{V} = \frac{h\,A\,(T_{ext} - T)}{V} \quad (7)$$

Where ρ is the broth density (kg/m^3), C_p is the specific heat (J/kg·K), h is the convective heat transfer coefficient, A is the surface area (m^2), T_{ext} is the jacket temperature, and T is the reactor internal temperature. The microbial heat generation is neglected due to the relatively small metabolic enthalpy changes compared to external thermal control systems (Pratiwi et al., 2015a).

Temperature also directly affects microbial activity, so an Arrhenius correction (Equation (8)) is applied to the specific growth rate to simulate the influence of thermal conditions on enzyme kinetics. This is implemented as a multiplicative factor.

$$f(T) = \exp\left(-\frac{E_a}{RT}\right) \quad (8)$$

Where E_a is the activation energy of microbial enzymes (typically 50–70 kJ/mol), and R is the universal gas constant. This ensures biologically plausible temperature-growth coupling.

This correction allows microbial growth and substrate utilization to be sensitive to deviations from the optimal temperature range. For thermophilic strains like *Thermotoga* or *Clostridium thermocellum*, this range is typically 55–70 °C (Gupta et al., 2024). For baseline simulation, temperature is held constant (55 °C), but varied parametrically to assess performance sensitivity. This allows the model to reveal trade-offs between growth acceleration at higher temperatures and enzyme denaturation or substrate instability.

2.5. Surfactant enhancement of hydrocarbon bioavailability

To model the enhanced availability of hydrophobic substrates, the simulation incorporates a surfactant effectiveness factor (α), which modifies the effective substrate concentration and the hydrogen yield from hexadecane. This factor represents the emulsification and dispersion effects of biosurfactants or additives like Tween 80, which have been experimentally shown to increase substrate surface area and improve microbial access (Veshareh et al., 2022).

In this model, the surfactant effect is implemented in two complementary ways. First, the effective concentration of hexadecane is scaled as $H_{eff} = \alpha$. H, where α ranges from 1.0 (no surfactant) to 12.0 (high enhancement), based on empirical findings from Veshareh et al. (2022) where up to 12 × improvement in hydrogen yield was reported when surfactant was added alongside glucose. Secondly, in scenarios where hexadecane acts as a secondary substrate in co-metabolism, the surfactant factor is applied directly to the yield coefficient. where $\beta \approx \alpha$ reflects the proportional gain in hydrogen productivity per mole of hexadecane (Equation (9)). These approaches allow the model to simulate not just microbial kinetics but also the physicochemical effect of emulsification on hydrocarbon utilization.

Including this factor is critical to accurately simulate reservoir conditions where oil-water interfaces dominate the microbial environment, and substrate accessibility is often the limiting factor for biohydrogen production. By varying α in the simulation from 1 to 12, the model reveals how surfactant-enhanced co-metabolism can overcome the bioavailability bottleneck and significantly improve both substrate utilization and total hydrogen yield. It also helps interpret trade-offs between surfactant cost and yield gains in future techno-economic assessments of MEHR systems.

$$Y_{H_2/H}^{effective} = \beta .\, Y_{H_2/H}^{base} \quad (9)$$

2.6. Parametric simulation design

To explore the influence of environmental and operational variables on biohydrogen production, a parametric simulation framework was developed using nested loops in Python. This structure allows systematic variation of key reactor conditions to observe their effects on hydrogen yield, substrate degradation, and microbial growth. The parameters selected include temperature (35, 45, 55, 70 °C), pressure (1, 10, 20, 40 atm), salinity (0, 15, 30, 50 g/L NaCl), and surfactant enhancement factor (α = 1, 3, 6, 12). Each of these variables is independently looped within the code, with the model equations solved iteratively using *scipy.integrate.odeint* for a fixed 24-h batch cycle. This approach enables a full-factorial sweep or targeted subset analysis, depending on the research focus.

For each simulation run, the model records time-resolved outputs for biomass concentration, substrate consumption (glucose and hexadecane), hydrogen accumulation (in mol and L), and system temperature. At the end of each loop, key summary statistics are computed, including final hydrogen yield (mol/mol substrate), hydrogen volume (L), yield enhancement (%), and remaining substrate concentrations. These results are saved in.csv format and visualized using matplotlib, allowing generation of time-series plots, bar charts, and visualizations. The simulation is configured to automatically track and compare performance across the parameter space, enabling efficient identification of optimal reactor conditions.

This parametric structure is essential to understanding the system's sensitivity to environmental stressors. For instance, simulations reveal that while hydrogen yield increases with temperature up to 55 °C, further increases reduce biomass due to thermal stress. Similarly, moderate salinity (15–30 g/L) can be tolerated by halophilic consortia, but performance sharply

declines at 50 g/L. The simulation also captures non-linear effects such as the diminishing returns of surfactant enhancement and how they interact with pressure-induced gas solubility. This comprehensive design makes the model not just a predictive tool, but also a framework for optimization and feasibility analysis in biohydrogen process engineering.

2.7. Initial conditions and model assumptions

To accurately represent the fermentation conditions typical of a reservoir-mimicking bioreactor, a standardized set of initial conditions was applied across all simulation runs. The initial biomass concentration was set at 0.1 g/L, representing a modest microbial inoculum reflective of start-up or in situ reservoir enrichment. Substrate concentrations were initialized at 10 mmol/L for glucose and 1.0 mmol/L for *n*-hexadecane, based on co-metabolic studies in dark fermentation systems (Veshareh et al., 2022). The base temperature was fixed at 55 °C, corresponding to optimal activity ranges for thermophilic anaerobes, while baseline pressure was set at 1 atm. Salinity was initialized at 0 g/L NaCl and increased in defined steps up to 50 g/L to simulate formation water conditions.

Several critical assumptions were made to simplify the model while retaining biological and physicochemical realism. First, the reactor was assumed to be perfectly mixed, with uniform concentrations of biomass, substrates, and products throughout the volume. This allowed the use of a lumped-parameter model without spatial gradients. Second, microbial decay was not included in the simulation timeframe, as the 24-h batch duration is typically dominated by growth and product formation. Third, the reactor was modeled as gas-tight, meaning no loss of hydrogen to the environment. Gas-liquid equilibrium was assumed to occur instantaneously, making hydrogen concentrations in the liquid and gas phases always conform to Henry's law.

Additionally, mass transfer limitations were not explicitly modeled, but diffusion constraints were indirectly represented through the surfactant enhancement factor and dual-substrate interactions. External temperature control was assumed to be effective and stable, based on typical lab- or reservoir-style thermal regulation via heating jackets or geothermal gradients. Energy input from microbial metabolism was considered negligible compared to external sources and thus excluded from the heat balance. These assumptions, though simplifying, are consistent with those used in prior computational and experimental studies of dark fermentation and provide a solid foundation for evaluating process behavior under a wide range of environmental conditions (Imai, 2024; Mamimin et al., 2015; Pratiwi et al., 2015b).

2.8. Model implementation and integration

The entire simulation framework was implemented in Python 3.11 using standard scientific computing libraries, including NumPy, SciPy, and Matplotlib. The system of ordinary differential equations (ODEs) describing biomass growth, substrate consumption, hydrogen generation, and temperature dynamics was numerically solved using *scipy.integrate.odeint*, which applies adaptive Runge-Kutta methods for stiff and non-stiff systems. Each ODE function was modularized within a *reactor_model.py file*, where growth kinetics were computed based on the current state variables and parameter set passed during runtime. The modular structure allows flexible extension to include additional pathways, such as VFAs or gas stripping, if needed. All model parameters and initial conditions were imported from a centralized configuration file (parameters.py) to ensure consistency across simulation runs.

For parametric studies, nested loops were implemented in a *simulation.py* script to automate simulation across all combinations of temperature, pressure, salinity, and surfactant factors. Each simulation run generated time-series data for hydrogen volume, biomass, substrate concentrations, and system temperature. Outputs were saved as.csv files and visualized using Matplotlib, enabling fast comparison of trends across different environmental scenarios. Code validation was performed by comparing model outputs under base conditions to benchmark results from Veshareh et al. (2022) for hexadecane fermentation and Gupta et al. (2024) for thermophilic glucose-based systems. This implementation ensures computational reproducibility, and the codebase is designed to be portable across systems for rapid prototyping and educational use.

2.9. Output metrics and visualization

The simulation framework produces both time-series data and summary metrics that describe system performance under each set of operating conditions. Key time-resolved outputs include biomass concentration (g/L), glucose and hexadecane levels (mmol/L), hydrogen accumulation (L), and reactor temperature (°C). These data allow visualization of the microbial growth curve, substrate degradation profiles, and cumulative hydrogen generation over the 24-h batch cycle. The simulation also tracks intermediate values such as hydrogen partial pressure and gas-liquid equilibrium concentration, which are used both in inhibition calculations and gas-phase performance analysis.

At the conclusion of each simulation run, a series of performance metrics is extracted. These include final hydrogen yield (mol H_2/mol substrate), hydrogen purity in the gas phase (%), biomass productivity (g/L), and substrate conversion efficiency for both glucose and hexadecane. These values are compiled into structured tables and visualized using bar plots, line charts, and 3D surface and contour plots to evaluate sensitivity to temperature, pressure, salinity, and surfactant factor. Visualizations are created using Matplotlib and Seaborn libraries in Python.

3. Results and discussion

3.1. Simulation outputs

The baseline simulation, conducted at 55 °C, 1 atm pressure, no salinity, and no surfactant enhancement ($\alpha = 1$), revealed a characteristic three-phase fermentation pattern. Biomass increased from 0.1 to 1.20 g/L over 24 h, with rapid exponential growth between 2 and 12 h. Glucose was almost completely consumed by hour 18, while *n*-hexadecane showed slower degradation, reaching about 50% conversion by the end of the batch as shown in Fig. 3. These results are consistent with co-metabolism behavior reported in literature, where easily fermentable substrates like glucose initiate microbial activity and enzyme expression that later enable slower hydrocarbon breakdown (Gupta et al., 2024; Veshareh et al., 2022).

Hydrogen production followed substrate degradation trends, reaching a cumulative yield of 4.34 L per batch. Most hydrogen was generated during the exponential biomass growth phase, corresponding to high glucose availability and metabolic activity. The final hydrogen purity in the gas phase reached 89.6%, with remaining volume attributed to water vapor and trace CO_2, consistent with typical dark fermentation gas profiles (Ghimire et al., 2015). These values align with the upper range of experimental yields reported in batch thermophilic studies, indicating that the simulated bioreactor under favorable conditions can closely replicate laboratory observations.

The differential conversion rates between glucose and hexadecane highlight the role of co-substrate design in optimizing

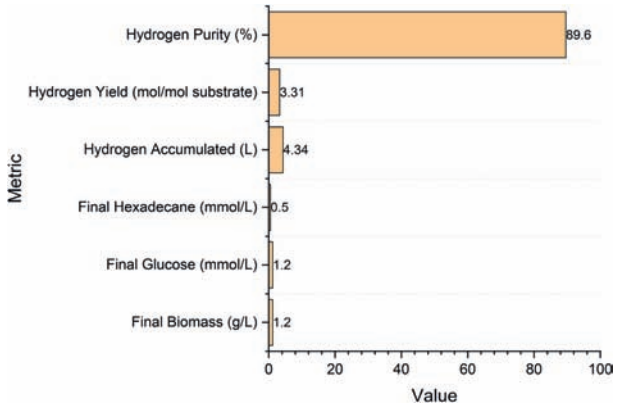


Fig. 3. Final bioreactor performance at 24 hours.

hydrogen yield. While glucose drove early-stage hydrogen evolution and biomass accumulation, hexadecane degradation contributed to sustained gas production later in the cycle as shown in Fig. 3. This is supported by experimental work by Veshareh et al. (2022), who reported delayed hexadecane utilization in the presence of glucose due to regulatory prioritization. The simulation confirms this dynamic, suggesting that substrate sequencing and controlled feeding strategies may enhance overall hydrogen productivity in both batch and continuous reactor systems.

3.2. Time-dependent system dynamics

The 24-h time-course simulation under baseline conditions (55 °C, 1 atm, 0 g/L NaCl, $\alpha = 1$) revealed clear temporal dynamics in microbial growth, substrate consumption, and hydrogen evolution. Biomass growth displayed a sigmoidal profile characteristic of batch fermentations, with a short lag phase (0–2 h), a rapid exponential phase (2–12 h), and a deceleration phase as substrates became limiting. Glucose depletion occurred more rapidly than hexadecane, with over 85% consumed within the first 12 h as shown in Fig. 4. In contrast, hexadecane exhibited a steady but slower decline, consistent with limited solubility and the requirement for inducible hydrocarbon-degrading enzymes. This sequential utilization supports the diauxic behavior reported in co-metabolism studies, where glucose is preferentially metabolized before transition to complex hydrocarbons.

Hydrogen production closely followed biomass growth and glucose degradation. The majority of hydrogen (approximately

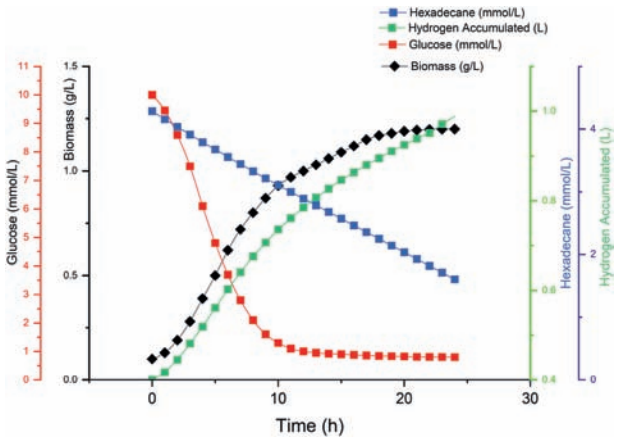


Fig. 4. Simulated Glucose utilization, Biomass production, hexadecane degradation and hydrogen accumulation with time.

80%) was produced between hours 4 and 14, coinciding with peak microbial activity. After glucose was largely exhausted, hydrogen production rate declined, although it continued at a slower rate due to ongoing hexadecane degradation. This trend reflects the lower hydrogen yield and slower metabolic conversion associated with hydrocarbons and underscores the importance of glucose in initiating and sustaining high metabolic throughput in dark fermentation. A final hydrogen yield of 3.31 mol/mol substrate was achieved in the co-substrate system, higher than yields reported for hexadecane-only fermentation (0.94 mol/mol), confirming the synergistic benefit of co-fermentation.

The temperature was held constant throughout the run, demonstrating external control effectiveness and supporting stable microbial kinetics. Notably, the hydrogen accumulation curve did not reach a plateau until near the 24-h mark, indicating that hexadecane may continue contributing to hydrogen production beyond a single batch cycle if biomass viability is maintained. This extended hydrogen evolution window suggests that reactor designs allowing controlled feeding or prolonged residence times could further improve yields.

3.3. Effect of temperature on hydrogen yield

Temperature significantly influenced both the rate and extent of hydrogen production, with the simulation confirming an optimal performance at 55 °C. At this temperature, the system achieved the highest cumulative hydrogen volume (4.34 L per batch) and the highest hydrogen yield of 3.31 mol/mol substrate. Increasing temperature from 35 °C to 55 °C enhanced microbial growth rate and substrate conversion efficiency due to improved enzymatic activity, as captured by the Arrhenius temperature dependence incorporated in the model (Kongjan et al., 2009; Pratiwi et al., 2015b; Rozanova et al., 2001). This is consistent with prior experimental work showing that thermophilic strains such as *Clostridium thermocellum* and *Thermotoga neapolitana* exhibit maximum hydrogen productivity in the 50–60 °C range (Gupta et al., 2024; Imai, 2024).

At 70 °C, a decline in both biomass and hydrogen yield was observed, despite higher kinetic rates predicted by the Arrhenius term. The drop in performance is attributed to enzyme instability or partial denaturation at supra-optimal temperatures, as well as increased water vapor saturation in the gas phase, which may dilute hydrogen purity. Final biomass was reduced to 0.82 g/L and hydrogen yield dropped to 2.94 mol/mol substrate at 70 °C, supporting the existence of a thermal threshold beyond which microbial metabolism becomes impaired as shown in Fig. 5. These findings align with experimental observations in dark fermentation, where hydrogen yields begin to decline above 65 °C, depending on the strain's thermotolerance (Ghimire et al., 2015).

Conversely, simulations at 35 °C and 45 °C showed slower biomass growth and delayed hydrogen evolution, reflecting the reduced enzymatic activity and metabolic sluggishness at suboptimal temperatures. The final hydrogen volumes at 35 °C and 45 °C were 2.85 L and 3.22 L respectively substantially lower than at 55 °C with longer lag phases and incomplete substrate degradation.

3.4. Effect of salinity on biomass growth and hydrogen yield

The simulation results revealed a clear inhibitory effect of salinity on both biomass growth and hydrogen production, consistent with microbial responses to osmotic stress. As NaCl concentration increased from 0 to 50 g/L, final biomass decreased from 1.45 g/L to 0.82 g/L, and hydrogen yield declined from 3.31 mol/mol to 1.92 mol/mol substrate as shown in Fig. 6. The

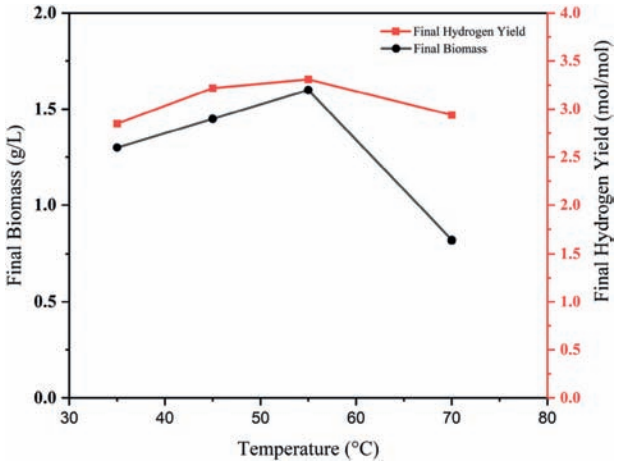


Fig. 5. Effect of temperature on final biomass and hydrogen yield.

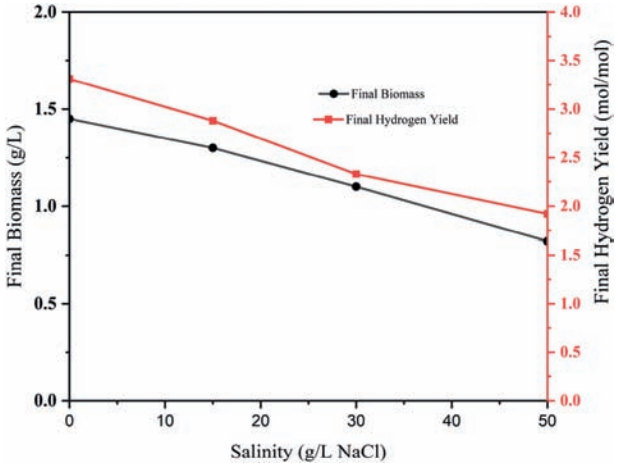


Fig. 6. Effect of Salinity on Biomass growth and Hydrogen yield.

most pronounced drop occurred beyond 30 g/L, suggesting a threshold above which even moderately halotolerant organisms face significant physiological stress. This trend matches known limits for hydrogen-producing consortia, where optimal performance is typically achieved at ≤20 g/L salinity, and inhibition intensifies beyond that range (Broussos et al., 2024; Younis and Mansour, 2024).

The inhibitory mechanism is twofold: high salinity creates osmotic imbalance, which disrupts microbial cell membranes, and also impairs enzyme function, reducing metabolic efficiency (Guo et al., 2014; Hosseini et al., 2022; Lawton et al., 2015). In the simulation, this was captured using a hyperbolic inhibition term with exponent n = 2n, which produced biologically realistic decay in growth rate with increasing salinity. Notably, glucose consumption slowed under higher salinity, but hexadecane degradation was even more limited likely due to its reliance on active transport mechanisms and secondary enzymatic pathways, which are more sensitive to ionic stress. The combined substrate degradation rate at 50 g/L was 40% lower than at 0 g/L, explaining the concurrent decline in hydrogen output.

3.5. Effect of pressure on hydrogen accumulation and purity

Pressure had a pronounced impact on hydrogen accumulation and purity in the simulated batch bioreactor. As pressure increased

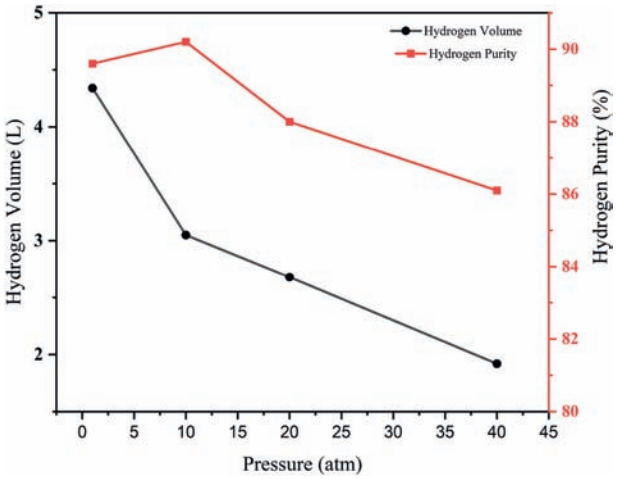


Fig. 7. Effect of pressure on Hydrogen volume and purity.

from 1 atm to 40 atm, the volume of hydrogen recovered in the gas phase declined from 4.34 L to 1.92 L, and hydrogen purity decreased from 89.6% to 86.1% as shown in Fig. 7. This reduction is attributable to enhanced hydrogen solubility in the aqueous phase under elevated pressures, as governed by Henry's Law. At higher pressures, more hydrogen remains dissolved in the liquid phase rather than accumulating in the gas phase, which diminishes recovery efficiency and amplifies product inhibition due to elevated internal P_{H2} (Kisielewska et al., 2015; Xiang et al., 2023).

The simulation linked this thermodynamic effect directly to microbial inhibition by incorporating a pressure-dependent hydrogen inhibition term in the growth rate equation. As pressure increased, the elevated dissolved H_2 concentrations suppressed hydrogenase activity, leading to reduced microbial growth and lower substrate conversion. This phenomenon has been experimentally observed in several anaerobic fermentative systems, where hydrogen accumulation beyond 0.6–0.8 atm in the headspace leads to feedback inhibition of NADH oxidation, a critical step in hydrogen metabolism (Ghimire et al., 2015). In the simulation, pressure effects were especially noticeable after 10 atm, indicating a nonlinear relationship between pressure and hydrogen inhibition.

From a reservoir engineering perspective, these findings highlight an operational trade-off: while higher pressure conditions better simulate subsurface environments, they also impose biological limitations. Field-scale strategies may need to incorporate periodic gas removal, depressurization, or selection of pressure-tolerant consortia to overcome inhibition and maintain performance.

3.6. Role of surfactant in hexadecane utilization

Simulation results revealed a strong positive effect of surfactant enhancement on *n*-hexadecane degradation and overall hydrogen yield. As the surfactant factor (α) was increased from 1 to 12, the final hexadecane concentration decreased from 0.80 mmol/L to 0.12 mmol/L, representing an 85% conversion. This enhanced degradation directly translated to higher hydrogen yields, which increased from 2.85 L at α = 1–4.91 L at α = 12, reflecting a 72.8% improvement in total gas production. The surfactant effect was modeled as a multiplicative enhancement in either substrate availability or hydrogen yield per mole hexadecane, capturing the role of emulsifiers in increasing surface area and phase contact. These results strongly validate the empirical findings of Veshareh

et al. (2022), who reported a 12-fold increase in hydrogen production with Tween 80 addition during hexadecane co-fermentation.

The surfactant effect was especially critical in later stages of the fermentation when glucose had been exhausted and hexadecane become the dominant carbon source. At low α values, hexadecane degradation stalled due to low bioavailability and phase separation, resulting in a plateau in hydrogen accumulation despite the presence of residual substrate. At higher α values, improved emulsification allowed sustained fermentation and continued hydrogen evolution beyond 18 h as shown in Fig. 8. This extended productivity window illustrates the potential of surfactant-assisted co-metabolism to maintain microbial activity and improve yield under diffusion-limited conditions often observed in subsurface environments.

While the simulation confirmed the efficacy of surfactant use, it also highlighted diminishing returns beyond $\alpha = 6$, where yield increases began to plateau. This suggests an optimal surfactant loading threshold beyond which additional emulsifier may not be cost-effective.

3.7. Substrate interaction and Co-metabolism

The simulation compared three substrate configurations: glucose-only, hexadecane-only, and glucose–hexadecane co-metabolism. Among them, the co-substrate system produced the highest hydrogen yield (3.31 mol/mol total substrate), followed by glucose-only (2.85 mol/mol) and hexadecane-only (0.94 mol/mol) as shown in Fig. 9. The superior performance of the dual-substrate condition can be attributed to the complementary metabolic roles of the two substrates. Glucose, being water-soluble and easily fermentable, rapidly supports microbial growth, while hexadecane, though slower to degrade, extends hydrogen production over time. This behavior aligns with known diauxic growth patterns, in which microorganisms prioritize simple sugars before inducing the enzymatic machinery required for complex hydrocarbon breakdown (Gupta et al., 2024; Veshareh et al., 2022).

In the glucose-only simulation, hydrogen production peaked early and plateaued after 12–14 h due to substrate depletion, with biomass reaching its maximum and then stabilizing. In contrast, the hexadecane-only system exhibited a delayed response with lower peak biomass (0.64 g/L) and reduced gas yield, reflecting the slow activation of hydrocarbon-degrading pathways and the substrate's low solubility. However, when both substrates were present, the model showed that early glucose metabolism accelerated

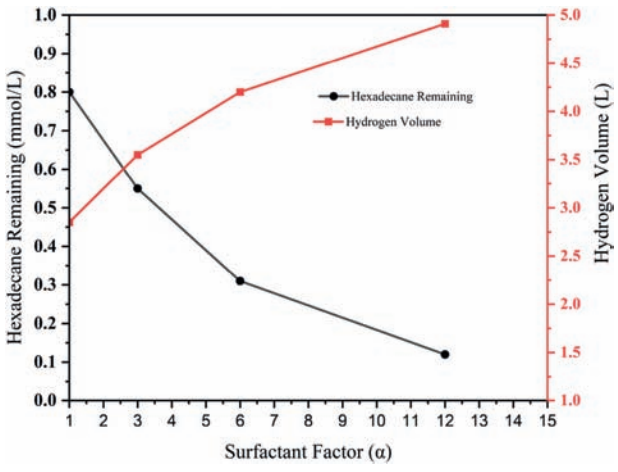


Fig. 8. Effect of Surfactant on Volume of hydrogen produced.

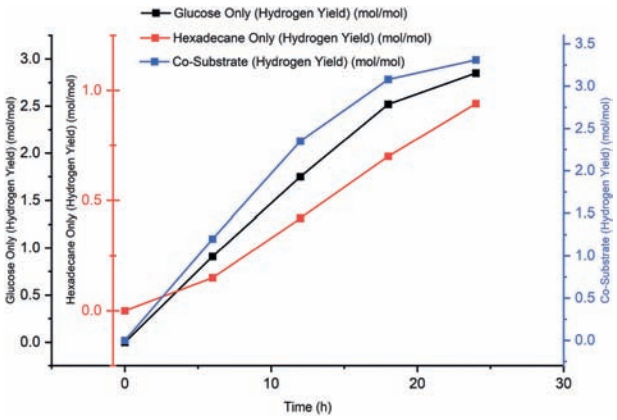


Fig. 9. Effect of Substrate Interaction and Co-Metabolism on hydrogen yield.

biomass buildup, which in turn increased the enzymatic capacity for hexadecane conversion during the latter half of the cycle. This resulted in an extended hydrogen production phase and more complete substrate utilization over 24 h.

These findings demonstrate the potential of substrate synergy in dark fermentation systems and reinforce co-metabolism as a viable strategy for enhancing hydrogen yields from residual hydrocarbons. In a reservoir context, where residual oil is not readily bioavailable, injecting co-substrates such as glucose, molasses, or other sugar-rich wastes could jumpstart microbial metabolism and improve system productivity.

3.8. Biological relevance and literature comparison

The simulated performance metrics obtained in this study including a maximum hydrogen yield of 4.34 L per batch, purity of 89.6%, and biomass levels exceeding 1.2 g/L fall within the ranges reported in the literature for thermophilic dark fermentation systems. For instance, Gupta et al. (2024) reported hydrogen yields of up to 3.2 mol/mol glucose in batch fermentations using *Clostridium thermocellum* at 55–60 °C, while Veshareh et al. (2022) achieved 0.88 mol/mol hexadecane in serum bottles with added glucose and Tween 80. The simulated values for glucose-only (2.85 mol/mol), hexadecane-only (0.94 mol/mol), and co-substrate (3.31 mol/mol) align well with these findings, confirming the biological credibility of the kinetic assumptions and pathway modeling.

Importantly, this study extends beyond existing work by quantifying the joint effects of pressure, salinity, and substrate interaction, none of which were addressed experimentally in prior research. For example, Veshareh's study used ambient pressure and did not simulate reservoir-like conditions. In contrast, this study revealed how pressures above 20 atm impair hydrogen release and how salinity above 30 g/L suppresses biomass growth, which gives critical insights for field deployment. Moreover, the incorporation of surfactant enhancement factors ($\alpha = 1$–12), inspired by Veshareh's reported 12 × yield boost, allowed quantification of hydrocarbon bioavailability in relation to substrate utilization and hydrogen productivity. These extensions bridge the gap between controlled laboratory studies and the complexity of subsurface environments.

Overall, this simulation provides a biologically grounded yet operationally expanded perspective on microbial hydrogen production. It validates observed trends from batch experiments, confirms the importance of co-substrate synergy, and highlights the limitations imposed by real-world thermodynamics. Most importantly, it provides a testable hypothesis for MEHR: that by

Table 1
Comparative overview of experimental biohydrogen production studies under varied conditions.

Study	Temperature (°C)	Pressure (atm)	Substrate	Microorganism	Max H_2 Yield	Max H_2 Production Rate	Key Features
This Study (Design)	35–70	40	Glucose + crude oil	Mixed anaerobes	2.33 mol/mol substrate	0.47 L/L·day	HPHT simulation; mimicking reservoir
Furqon et al. (2024)	30	1	DEPOME (dark fermented POME effluent)	*R. palustris*	0.27 mol/mol glucose	0.15	Photo-fermentation; LED light
Veshareh et al. (2022)	70	1	Crude oil + Tween 80 + Glucose	*Thermotoga* strains	5.7 mmol/L	0.28 mmol/L·h	In-situ simulation using reservoir-isolated strains
Wang et al. (2022)	35	1	Vegetable waste	Enriched microflora	151.7 mL/g VS	~0.42 L/L·day	Thermophilic batch fermentation
Zhang et al. (2008)	35	1	Glucose	Biofilm consortium	~1.7 mol/mol	~6.8 L/L·h (high-rate reactor)	Continuous system with granular sludge
Lay et al. (2012)	37–55	1	Waste sludge	Mixed culture	7.8 mmol	–	Sludge-based feedstock system

manipulating temperature, pressure, salinity, and surfactant loading, it is possible to engineer a stable and productive bioreactor environment within depleted hydrocarbon reservoirs. This opens a pathway for using simulation to guide experimental design and ultimately scale dark fermentation from lab-scale to field-ready energy systems. Table 1 presents a comparative analysis of selected experimental studies on biohydrogen production, highlighting the diversity of operational conditions, substrates, microbial systems, and reactor configurations. The studies include a range of temperatures, pressures, and substrate types; from glucose and crude oil to complex waste materials and employ various microbial consortia, including both pure and mixed cultures. This comparison underscores advancements in biohydrogen yield optimization and the exploration of HPHT environments to mimic subsurface reservoir conditions.

4. Limitations and future modeling directions

Assumption of instantaneous gas-liquid equilibrium and perfect headspace sealing. In practice, gas accumulation is affected by mass transfer resistance, leakage, and solubility lag especially at higher pressures and salinities. Also, temperature was assumed to be externally controlled and spatially uniform, which is often not the case in large-scale or geothermal environments where thermal gradients may develop. These assumptions, while enabling computational tractability, does not fully describe the ideal situation of the reservoir properties. Therefore, future modeling work should incorporate reactive transport models that include spatial gradients in pressure, temperature, and concentration, as well as multi-species dynamics to better capture microbial interactions in co-culture systems. Incorporating VFA accumulation, gas backpressure effects, and energy balances with internal heat generation would further improve predictive accuracy. Validation of simulation outputs with laboratory experiments especially under controlled salinity and pressure is also essential to confirm model fidelity. Ultimately, integrating this simulation framework with reservoir-scale geological models will enable the design of field-ready MEHR systems, contributing to the strategic repurposing of depleted reservoirs for clean energy generation.

5. Conclusion

This study presents a comprehensive numerical simulation of microbial hydrogen production under HPHT conditions representative of depleted hydrocarbon reservoirs. The developed model integrates dual-substrate fermentation kinetics, inhibition mechanisms, surfactant-enhanced hydrocarbon bioavailability, and thermodynamic gas-phase behavior to capture the complex interplay of microbial activity and environmental constraints. Simulation results underscore the potential of glucose and *n*-hexadecane co-metabolism for sustained hydrogen evolution, with optimal performance observed at 55 °C and atmospheric pressure. Elevated pressure and salinity were found to inhibit both biomass growth and hydrogen accumulation, while surfactant addition significantly improved hydrocarbon substrate utilization and overall gas yield. The parametric framework implemented in Python provides a flexible tool for evaluating MEHR strategies, enabling rapid assessment of operational conditions prior to field trials. By simulating reservoir-relevant thermophysical conditions, this work bridges the gap between laboratory-scale observations and field-scale feasibility assessments. Future efforts should focus on model calibration with experimental HPHT fermentation data, integration with multiphase flow simulators, and extension to continuous or in situ reservoir configurations. Overall, the simulation platform offers a valuable foundation for optimizing biohydrogen production in repurposed subsurface energy systems.

CRediT authorship contribution statement

David Abutu: Resources, Methodology, Investigation, Conceptualization. **Peter Ikechukwu Nwaichi:** Visualization, Validation, Formal analysis. **Chika Umunnawuike:** Validation, Resources, Project administration. **Francis Nyah:** Validation, Resources, Data curation. **Barima Money:** Visualization, Software, Resources. **Hafizuddin Wan Yussof:** Supervision, Resources, Project administration. **Augustine Agi:** Conceptualization, Project administration, Supervision.

Funding

This research was funded by Petronas Malaysia under grant number UIC240814.

Declaration of competing interest

The authors declare that they have no competing interests.

Abbreviations

MEHR	Microbial-Enhanced Hydrogen Recovery
HRT	Hydraulic Retention Time
CFD	Computational Fluid Dynamics
PID	Proportional-Integral-Derivative (Control System)
OD600	Optical Density at 600 nm
GC-TCD	Gas Chromatography with Thermal Conductivity Detector

Appendix A. Supplementary data

Supplementary data to this article can be found online at https://doi.org/10.1016/j.ptlrs.2025.07.006.

Appendix A. Simulation Parameters and Constants

Symbol	Unit	Description	Typical Value/Range	Source/Assumption
S	mol/L	Substrate concentration (glucose, hexadecane)	Glucose: 10 mmol/L; Hexadecane: 1 mmol/L	Assumed; Veshareh et al. (2022)
G,H_G	mol/L	Concentration of glucose (G) or hexadecane (H)	G: 10 mmol/L, H: 1 mmol/L	Assumed based on co-metabolism setup
X	g/L	Biomass concentration	0.1–1.5 g/L	Gupta et al. (2024)
μ	h^{-1}	Specific microbial growth rate	0.2–0.6 h^{-1}	Literature range (Gupta et al., 2024)
μmax	h^{-1}	Maximum growth rate	0.3–0.6 h^{-1}	Literature (Clostridium, Thermotoga)
K_s	mol/L	Half-saturation constant	0.05–0.2 mmol/L	Typical for glucose-fermenting strains
K_I	mol/L	Product inhibition constant	0.1–0.5 mmol/L H_2	Assumed; fitted to match VFA inhibition
$Y_{X/S}$	g/g	Biomass yield per substrate	0.4–0.7 g biomass/g glucose	Experimental studies (various)
$Y_{H2/S}$	mol/mol	Hydrogen yield per mol substrate	Glucose: 2–3.5; Hexadecane: 0.1–0.94	Veshareh et al. (2022)
T	°C or K	Reactor temperature	35, 45, 55, 70 °C	Parameter loop; literature benchmark
Text	°C or K	External control temperature	Same as TTT	Controlled via heating jacket
ρ	kg/m^3	Liquid density	1000 kg/m^3	Assumed (water-like broth)
C_p	J/kg·K	Specific heat capacity	4184 J/kg·K	Assumed (water)
h	$W/m^2·K$	Heat transfer coefficient	10–50 $W/m^2·K$	Literature for natural convection
A	m^2	Heat transfer surface area	Depends on reactor size	Design-based
V	L	Reactor volume	1.0 L (lab-scale)	Assumed
Q	W	Heat transfer rate	–	Calculated from energy equation
H_c	mol/L·atm	Henry's constant (for H_2)	7.8×10^{-4} mol/L·atm	At 25 °C; corrected for T
P	atm	Operating pressure	1–40 atm	Simulation range; reservoir mimic
R	L·atm/mol·K	Ideal gas constant	0.0821	Constant
n_{H2}	mol	Total hydrogen produced	–	Integration result
V_{H2}	L	Volume of hydrogen gas	–	Calculated using ideal gas law
f(T)	–	Temperature correction (Arrhenius)	exp(−Ea/RT)	Modeled explicitly
E_a	kJ/mol	Activation energy for microbial enzymes	50–70 kJ/mol	Literature range for thermophiles

Appendix B

Python Simulation Code Structure and Equation Mapping.

This appendix describes the structure of the Python-based simulation developed to model microbial hydrogen production under high-temperature, high-pressure, and saline conditions in a batch bioreactor. The simulation solves a system of ODEs representing biomass growth, substrate consumption, hydrogen production, and thermal dynamics. All governing equations are described in the methodology section of the manuscript.

B.1 Code Overview.

The simulation is implemented in a modular Python script consisting of the following components:

Module	Function
parameters.py	Contains constants, units, yield coefficients, inhibition parameters
kinetics.py	Implements Monod and inhibition equations for microbial growth
odemodel.py	Defines the coupled differential equations
simulation.py	Runs the time integration and parametric loops
visualization.py	Handles plotting of results (hydrogen yield, substrate profiles, temperature)
main.py	Master script that executes batch runs across the parametric grid

References

Aghajani Delavar, M., Wang, J., 2022. Modeling microbial growth of dynamic membrane in a biohydrogen production bioreactor. Int. J. Hydrogen Energy 47 (12), 7666–7681. https://doi.org/10.1016/j.ijhydene.2021.12.090.

Basak, N., Jana, A.K., Das, D., 2022. Photofermentative biohydrogen generation from organic acids by *Rhodobacter sphaeroides* O.U.001: computational fluid dynamics modeling of hydrodynamics and temperature. Biotechnol. Appl. Biochem. 69 (2), 783–797. https://doi.org/10.1002/bab.2151.

Broussos, P.-I., Romanos, G.E., Stamatakis, K., 2024. Salt and heat stress enhances hydrogen production in Cyanobacteria. Photosynth. Res. 161 (1–2), 117–125. https://doi.org/10.1007/s11120-024-01098-2.

Furqon, P., Purwanto, Y.A., Setiawan, R.P.A., Susilo, B., 2024. Biohydrogen production from DEPOME (dark fermented effluent palm oil mill effluent) via photofermentation utilizing indigenous bacteria. International Journal of Hydrogen Energy 56, 323–329. https://doi.org/10.1016/j.ijhydene.2023.12.127.

Ghimire, A., Frunzo, L., Pirozzi, F., Trably, E., Escudie, R., Lens, P.N.L., Esposito, G., 2015. A review on dark fermentative biohydrogen production from organic biomass: process parameters and use of by-products. Appl. Energy 144, 73–95. https://doi.org/10.1016/j.apenergy.2015.01.045.

Goria, K., Kothari, R., Singh, H.M., Singh, A., Tyagi, V.V., 2022. Biohydrogen: potential applications, approaches, and hurdles to overcome. Handbook of Biofuels. Elsevier 399–418. https://doi.org/10.1016/B978-0-12-822810-4.00020-8.

Guo, L., Zong, Y., Lu, M., Zhang, J., 2014. Effect of different substrate concentrations and salinity on hydrogen production from mariculture organic waste (MOW). Int. J. Hydrogen Energy 39 (2), 736–743. https://doi.org/10.1016/j.ijhydene.2013.10.127.

Gupta, S., Fernandes, A., Lopes, A., Grasa, L., Salafranca, J., 2024. Microbes and parameters influencing dark fermentation for hydrogen production. Appl. Sci. 14 (23), 10789. https://doi.org/10.3390/app142310789.

Hosseini, M., Fahimpour, J., Ali, M., Keshavarz, A., Iglauer, S., 2022. H2−brine interfacial tension as a function of salinity, temperature, and pressure; implications for hydrogen geo-storage. J. Petrol. Sci. Eng. 213, 110441. https://doi.org/10.1016/j.petrol.2022.110441.

Imai, T., 2024. Thermotolerance and hydrogen production potential of salt-tolerant microbial communities from salt fields. Chiang Mai J. Sci. 51 (6), 1–15. https://doi.org/10.12982/CMJS.2024.107.

Jain, R., Panwar, N.L., Jain, S.K., Gupta, T., Agarwal, C., Meena, S.S., 2024. Biohydrogen production through dark fermentation: an overview. Biomass Convers. Biorefinery. 14 (12), 12699–12724. https://doi.org/10.1007/s13399-022-03282-7.

Kaydouh, M.-N., El Hassan, N., 2022. Thermodynamic simulation of the co-gasification of biomass and plastic waste for hydrogen-rich syngas production. Results Eng. 16, 100771. https://doi.org/10.1016/j.rineng.2022.100771.

Kisielewska, M., Dębowski, M., Zieliński, M., 2015. Improvement of biohydrogen production using a reduced pressure fermentation. Bioproc. Biosyst. Eng. 38 (10), 1925–1933. https://doi.org/10.1007/s00449-015-1434-3.

Kongjan, P., Min, B., Angelidaki, I., 2009. Biohydrogen production from xylose at extreme thermophilic temperatures (70°C) by mixed culture fermentation. Water Res. 43 (5), 1414–1424. https://doi.org/10.1016/j.watres.2008.12.016.

Lawton, R.J., de Nys, R., Magnusson, M.E., Paul, N.A., 2015. The effect of salinity on the biomass productivity, protein and lipid composition of a freshwater macroalga. Algal Res. 12, 213–220. https://doi.org/10.1016/j.algal.2015.09.001.

Lay, C.-H., Sung, I.-Y., Kumar, G., Chu, C.-Y., Chen, C.-C., Lin, C.-Y., 2012. Optimizing biohydrogen production from mushroom cultivation waste using anaerobic mixed cultures. International Journal of Hydrogen Energy 37 (21), 16473–16478. https://doi.org/10.1016/j.ijhydene.2012.02.135.

Li, W., Li, S., M. Abed, A., Ayed, H., Khadimallah, M.A., Deifalla, A., Lee, V.F., 2024. Enhancing green hydrogen production via improvement of an integrated double flash geothermal cycle; Multi-criteria optimization and exergo-

environmental evaluation. Case Stud. Therm. Eng. 59, 104538. https://doi.org/10.1016/j.csite.2024.104538.
Mamimin, C., Singkhala, A., Kongjan, P., Suraraksa, B., Prasertsan, P., Imai, T., O-Thong, S., 2015. Two-stage thermophilic fermentation and mesophilic methanogen process for biohythane production from palm oil mill effluent. Int. J. Hydrogen Energy 40 (19), 6319–6328. https://doi.org/10.1016/j.ijhydene.2015.03.068.
Medina, O.E., Gallego, J.F., Moncayo-Riascos, I., Lysyy, M., Benjumea, P.N., Cortés, F. B., Franco, C.A., 2024. Salinity influence on underground hydrogen storage: insights from molecular dynamics and pore-scale analysis. Int. J. Hydrogen Energy 60, 959–975. https://doi.org/10.1016/j.ijhydene.2024.02.073.
Nadal-Rey, G., McClure, D.D., Kavanagh, J.M., Cassells, B., Cornelissen, S., Fletcher, D. F., Gernaey, K.V., 2022. Computational fluid dynamics modelling of hydrodynamics, mixing and oxygen transfer in industrial bioreactors with Newtonian broths. Biochem. Eng. J. 177, 108265. https://doi.org/10.1016/j.bej.2021.108265.
Pratiwi, B., RamdlanKirom, M., FauziIskandar, R., 2015a. Design of temperature control based fuzzy logic for substrate in thermophilic hydrogen reactor. In: 2015 International Conference on Control, Electronics, Renewable Energy and Communications (ICCEREC), pp. 85–90. https://doi.org/10.1109/ICCEREC.2015.7337060.
Pratiwi, B., RamdlanKirom, M., FauziIskandar, R., 2015b. Design of temperature control based fuzzy logic for substrate in thermophilic hydrogen reactor. In: 2015 International Conference on Control, Electronics, Renewable Energy and Communications (ICCEREC), pp. 85–90. https://doi.org/10.1109/ICCEREC.2015.7337060.
Rozanova, E.P., Borzenkov, I.A., Tarasov, A.L., Suntsova, L.A., Dong, Ch L., Belyaev, S. S., Ivanov, M.V., 2001. Microbiological processes in a high-temperature oil field. Microbiology. Microbiology 70 (1), 102–110. https://doi.org/10.1023/A:1004809308305.
Sarangi, P.K., Nanda, S., 2020. Biohydrogen production through dark fermentation. Chem. Eng. Technol. 43 (4), 601–612. https://doi.org/10.1002/ceat.201900452.
Umunnawuike, C., Mahat, S.Q.A., Nwaichi, P.I., Money, B., Agi, A., 2024. Biohydrogen production for sustainable energy transition: a bibliometric and systematic review of the reaction mechanisms, challenges, knowledge gaps and emerging trends. Biomass Bioenergy 188, 107345. https://doi.org/10.1016/j.biombioe.2024.107345.
Veshareh, M.J., Poulsen, M., Nick, H.M., Feilberg, K.L., Eftekhari, A.A., Dopffel, N., 2022. The light in the dark: In-situ biorefinement of crude oil to hydrogen using typical oil reservoir Thermotoga strains. Int. J. Hydrogen Energy 47 (8), 5101–5110. https://doi.org/10.1016/j.ijhydene.2021.11.118.
Vilcáez, J., Chowdhury, E., 2025. Biogenic hydrogen production from oil hydrocarbons at geological carbon storage conditions. Energy Convers. Manag. 325, 119438. https://doi.org/10.1016/j.enconman.2024.119438.
Wang, N., Chui, C., Zhang, S., Liu, Q., Li, B., Shi, J., Liu, L., 2022. Hydrogen Production by the Thermophilic Dry Anaerobic Co-Fermentation of Food Waste Utilizing Garden Waste or Kitchen Waste as Co-Substrate. Sustainability 14 (12), 7367. https://doi.org/10.3390/su14127367.
Wu, L., Hou, Z.-M., Luo, Z.-F., Fang, Y.-L., Huang, L.-C., Wu, X.-N., Chen, Q.-J., Wang, Q.-C., 2024. Impacts of microbial interactions on underground hydrogen storage in porous media: a comprehensive review of experimental, numerical, and field studies. Pet. Sci. 21 (6), 4067–4099. https://doi.org/10.1016/j.petsci.2024.08.015.
Xiang, G., Zhang, H., Li, Y., Liu, H., Zhang, Z., Lu, C., Zhang, Q., 2023. Enhancing biohydrogen yield from corn stover by photo fermentation via adjusting photobioreactor headspace pressure. Bioresour. Technol. 369, 128388. https://doi.org/10.1016/j.biortech.2022.128388.
Younis, A.A., Mansour, M.M.F., 2024. Hydrogen sulfide-mitigated salinity stress impact in sunflower seedlings was associated with improved photosynthesis performance and osmoregulation. BMC Plant Biol. 24 (1), 422. https://doi.org/10.1186/s12870-024-05071-y.
Zhang, Z., Show, K., Tay, J., Liang, D., Lee, D., 2008. Biohydrogen production with anaerobic fluidized bed reactors—A comparison of biofilm-based and granule-based systems. International Journal of Hydrogen Energy 33 (5), 1559–1564. https://doi.org/10.1016/j.ijhydene.2007.09.048.
Ziara, R.M.M., Miller, D.N., Subbiah, J., Dvorak, B.I., 2019. Lactate wastewater dark fermentation: the effect of temperature and initial pH on biohydrogen production and microbial community. Int. J. Hydrogen Energy 44 (2), 661–673. https://doi.org/10.1016/j.ijhydene.2018.11.045.